DECODING THE DOMINO:
THE DARK SIDE OF IAPETUS

Tobias C. Owen [1]
University of Hawaii Institute for Astronomy
2680 Woodlawn Drive, Honolulu, HI 96822
808-956-8007 Voice; 808-956-9580 FAX
E-mail: owen@ifa.hawaii.edu

Dale P. Cruikshank [1]
NASA Ames Research Center
Moffett Field, CA 94035-1000
dale@ssa1.arc.nasa.gov

C. M. Dalle Ore
SETI Institute and NASA Ames Research Center
Moffett Field, CA 94035-1000
cdo@misty.arc.nasa.gov

T. R. Geballe [2]
Gemini Telescope
670 N. A'ohoku Place, Hilo, HI 96720
tgeballe@gemini.edu

T. L. Roush
NASA Ames Research Center
Moffett Field, CA 94035-1000
troush@mail.arc.nasa.gov

C. de Bergh [1]
Observatoire de Paris
5 Place Jules Janssen, 92195 Meudon Cedex, France
debergh@obspm.fr

Roland Meier [1]
University of Hawaii Institute for Astronomy
2680 Woodlawn Drive, Honolulu, HI 96822

Yvonne J. Pendleton
NASA Ames Research Center, Moffett Field, CA 94035-1000
ypendleton@mail.arc.nasa.gov

Bishun N. Khare
SETI Institute and NASA Ames Research Center
Moffett Field, CA 94035-1000
bkhare@mail.arc.nasa.gov

[1] Guest observer, UKIRT

[2] Affiliation at the time of the observational work: Joint Astronomy Centre, 660 N. A'ohoku Pl., University Park, Hilo, HI 96720

Number of Pages   37
Number of Figures   12
Number of Tables   2

Received:_____   Revised:_____

Running Head
        The Dark Side of Iapetus

Send Correspondence to
        Tobias Owen
        University of Hawaii
        Institute for Astronomy
        2680 Woodlawn Drive
        Honolulu, HI 96822

        Phone 808-956-8007
        FAX 808-956-9580
        e-mail: owen@ifa.hawaii.edu

ABSTRACT

We present new spectra of the leading and trailing hemispheres of Iapetus from 2.4 to 3.8 μm. We have combined the leading hemisphere spectra with previous observations by others to construct a composite spectrum of the dark side (leading) hemisphere from 0.3 to 3.8 μm. We review attempts to deduce the composition of the dark material from previously available spectrophotometry. None of them (numbering more than 20 million!) leads to a synthetic spectrum that matches the new data. An intimate mixture of water ice, amorphous carbon and a nitrogen-rich organic compound (modeled here as Triton tholin) can fit the entire composite dark side spectrum. Observations in this spectral region have not revealed this mix of material on any other object observed thus far. We propose that this dark material may have originated on Titan, where atmospheric photochemistry has been producing nitrogen-rich organic compounds for 4.5 GY.

1.   INTRODUCTION

Despite numerous Earth-based investigations and two Voyager flybys, the composition and origin of the dark material coating the leading hemisphere of Iapetus remain unknown. Cassini (1673) described the basic problem after his discovery of this enigmatic satellite of Saturn in 1671: "...one part of [Iapetus] surface is not so capable of reflecting to us the light of the Sun which maketh it visible, as the other part is...". Indeed it isn't. Analysis of Voyager images by Squyres et al. (1984) revealed that the extreme difference in visible reflectivity between the two hemispheres amounts to a factor between 10 and 20, by far the largest such asymmetry in the solar system. This extreme difference in the reflectivity of the two hemispheres is also illustrated by the difference in their thermal radiation. The observed 20-μm flux from Iapetus reaches a maximum when the satellite is visibly faintest (eastern elongation), and has its minimum when Iapetus is at its brightest (western elongation) (Morrison et al. 1975).

How did this happen? Why only on Iapetus? And what is the dark material that makes the leading hemisphere "...not so capable of reflecting to us the light of the sun ..." ? Is it similar to any of the dark coatings on other small bodies in the outer solar system or is it unique to Iapetus?

Previous investigations have attempted to discriminate between internal and external mechanisms for forming this dark covering. On the basis of a new analysis of Voyager images, Buratti and Mosher (1995) have convincingly argued in favor of an external process, but there are still many possibilities: e.g., *deposition* of dust from Phoebe (Soter 1974; Cruikshank et al. 1983; Hamilton 1997; Jarvis et al. 2000) as well as *erosion* by Phoebe dust, which could leave a lag deposit of organics mixed with hydrated silicates (Bell et al. 1985) or reveal an underlying layer of extruded organics (Wilson and Sagan 1995, 1996). Or perhaps it is not Phoebe dust but interplanetary dust that is the eroding agent (Cook and Franklin 1970; Wilson and Sagan 1996). Among suggested components and compositions for the dark coating, we can mention a hydrated silicate mineral mixed with a small amount of water frost, darkened by an admixture of carbonaceous matter (Lebofsky et al. 1982), simulated meteoritic organic polymers ("ultra-carbonaceous" material) mixed with hydrated silicates (Bell et al. 1985), organic polymers containing – C $\equiv$ N (Cruikshank et al. 1991), Murchison meteorite residue

(acid insoluble), water ice and poly HCN (Wilson and Sagan 1995), and hydrated silicates that contain iron alteration minerals, mixed with organics and ice (Vilas et al. 1996).

Vilas et al. (1996) based their suggestion of the presence of iron alteration minerals on the discovery of a discrete absorption feature at 0.67 μm in the dark side spectrum that they attributed to the $^6A_1 \rightarrow {}^4T_2$ (G) Fe^{3+} charge transfer transition. They recognized that these minerals could only be one component of the coating material and confirmed the sharp rise in reflectance with wavelength in the visible range that is characteristic of many dark organic compounds. What are these compounds?

Wilson and Sagan (1995) reported that they examined approximately 20 million possible combinations of six plausible components, including poly-HCN, to obtain the best fit to the Bell et al. (1985) spectrum of the Iapetus dark material. Yet they noted that "...other mixture types and compositions also produce very good fits..." provided that poly-HCN was always included to give the red slope required to match the visible spectrum. They cautioned that "...in the absence of spectral features, compositions are being selected based on absorption slopes for which uniqueness [of model fits] cannot be claimed."

In fact there is a very strong absorption feature in the dark side spectrum at 3.0 μm , discovered at low spectral resolution by Lebofsky et al. (1982) who deduced the composition given above. Wilson and Sagan (1996) did not extend their models to this spectral region, although they did illustrate the wavelength dependence of the absorption coefficients for their model components out to 5 μm.

It is precisely the frustrating lack of diagnostic features in the dark side spectrum and the diagnostic potential of the 2.85 − 4.85 μm region that stimulated the present investigation. During the last five years, we have used the cooled grating spectrometer (CGS4) at the United Kingdom Infrared Telescope (UKIRT) to obtain spectra of the Iapetus darkside with higher spectral resolution and signal to noise than has been possible heretofore. Our goal has been to find and identify discrete absorptions in the spectrum in order to explain the dark, reddish organic material that appears to be an essential component of all models suggested to date. We also hoped to be able to say something useful about the other components that various authors have suggested.

2. OBSERVATIONS

The first step in our investigation was to record the dark side spectrum in the region $2.0 - 2.5$ μm to test for the presence of an absorption at 2.2 μm reported by Cruikshank et al. (1991). It was this absorption that led these authors to the original suggestion that poly HCN or some other - C ≡ N containing compound is a major contributor to the dark side material. Cruikshank et al. (1991) showed that a 2.2 μm absorption is found in laboratory reflection spectra of poly HCN and some organic compounds known as "tholins" which are produced by the irradiation of mixtures of N_2 and CH_4. They attributed this feature to the first overtone of the - C ≡ N stretching vibration that occurs near 4.6 μm.

However, we found no evidence of the 2.2 μm absorption in the CGS4 spectra of the dark side of Iapetus (Owen et al. 1995). This absorption is also absent in newly recorded spectra of five of the other objects listed as carriers of this feature by Cruikshank et al. (1991): four asteroids and the rings of Uranus; (Luu et al. 1994; Barucci et al. 1994; Dumas et al. 1998) the two comet nuclei cannot be reobserved in the foreseeable future. The cited references include studies of many other dark asteroids in this same spectral region, again with no evidence of any diagnostic absorptions, with sole exception of 5145 Pholus, whose spectrum was recently interpreted by Cruikshank et al. (1998a). (The 2.27 μm feature in the spectrum of Pholus published by Cruikshank et al. is also seen in independently obtained data by Luu et al. [1994]). While the spectrum of this Centaur contains several absorptions, none of them occurs at 2.2 μm. Evidently the 2.2 μm feature appearing in the spectra collected by Cruikshank et al. (1991) was some type of instrumental artifact that successfully resisted removal during data analysis. Thus the inability of the Wilson and Sagan (1996) models of Iapetus dark side material to reproduce this feature – despite the authors consistent inclusion of poly HCN – is not an argument against these models, as Wilson and Sagan (1996) correctly surmised.

The next step in our study was to examine the $2.8 - 4.0$ μm spectral window where Lebofsky et al. (1982) had found the very strong 3 μm absorption band noted above, which was confirmed by Cruikshank et al. (1983). This proved to be a difficult undertaking, foiled by three years of successive bouts of bad weather and/or instrument problems. We finally succeeded in recording the region covering $2.8 - 3.4$ μm in

October 1997, as documented in Table I. We subsequently extended these observations to 3.8 μm and added comparison spectra of the bright side (trailing hemisphere) of Iapetus (Table 1).

TABLE 1

2.1 NEW OBSERVATIONS AND DATA REDUCTION

Spectra of the leading side of Iapetus were obtained at UKIRT on UT 1997 October 6, approximately one-half day after eastern elongation; those of the trailing side were obtained on 1998 December 18, within a few hours of western elongation. A log of the observations is provided in Table 1. For both sets of astronomical observations the 40 lines/mm grating of CGS4 was used in first order with a 1.2" slit (aligned east-west), yielding a resolution of 0.005 μm at all wavelengths. For the purpose of flux calibration and removal of telluric and solar features, spectra of a near-solar analogue star, BS 582 (G2IV, V = 5.88; Te = 5600 and L = 4.30 were assumed), were recorded before and/or after those of Iapetus in order to match the mean airmasses of the star and Iapetus to within a few percent in each spectral segment. Wavelength calibration was obtained from measurements of argon arc lines in first and second order and is accurate to better than 0.001 μm .

The flux- and wavelength-calibrated spectral segments listed in Table 1 were then scaled and merged to provide contiguous spectra at eastern and western elongations, the 2.8 – 3.8 μm sections of which are shown in Figure 1, smoothed to a resolution of 0.02 μm. Small (< 20%) scaling adjustments of the spectra were required in order for the segments to match one another. No adjustments were made for the slightly different Sun-Saturn and Saturn-Earth distances of the two spectra. We estimate that the flux levels of these spectra are accurate to ± 20%. Figure 1 reveals that at 3-4 μm the leading hemisphere, or "dark side" is brighter than the trailing hemisphere by factors ranging from ~1.3 to ~5. Both spectra show a strong absorption around 3.0 μm, a rise to a peak near 3.6 μm, and a decrease at longer wavelengths. Both also show an emission bump at ~3.10 μm, which is much less pronounced on the leading hemisphere.

FIGURE 1

2.2 CONSTRUCTION OF THE COMPOSITE SPECTRUM

To enable a comprehensive analysis of the dark matter on Iapetus, we have combined our new data from the near infrared 2.8 – 3.8 μm region with previous observations at shorter wavelengths to produce the spectrum shown in Figure 2, which extends from 0.3 – 3.8 μm .

FIGURE 2

The spectrum of Iapetus in the region 0.32 to 2.42 μm published by Bell et al. (1985) was produced by combining two data sets. The first, covering 0.32 to 0.93 μm, was obtained with a set of narrow-band interference filters at the satellite's eastern elongation of 21-22 May 1979 (Cruikshank et al. 1983). The second data set covered 0.8 to 2.6 μm, and was obtained with two circular-variable interference filters on 11 February 1982 (Bell et al. 1985). Using a linear mixing model and spectra of the high albedo hemisphere of Iapetus, Bell et al. (1985) removed from the dark hemisphere spectrum a composition corresponding to the fractional contribution of the high albedo hemisphere visible at eastern elongation. This produced the final spectrum in their Figure 5, which is the reflectance of Iapetus' dark surface unit without polar cap contamination. This spectrum is satisfactorily matched by Voyager photometry in the short wavelength range (Thomas et al. 1982). More recent data by Vilas et al. (1996), covering the interval 0.30 to 0.89 μm , included in the spectrum shown in Figure 2, are slightly more steeply sloped toward the longer wavelengths than the Bell et al. data, but overall the match is fairly good.

In the present work, we have elected to use the Bell et al. (1985) spectrum of the low-albedo hemisphere without any attempt to remove the water ice signature that might represent contamination from the polar regions (their Figure 2). Thus, the spectrum which we have modeled includes H_2O ice absorption bands at 1.5, 2.0 and 2.4-2.5 μm .

In our presentations of those data, we show a continuous line passing through the individual data points in Figure 2 of Bell et al. (1985).

The short wavelength limit of the new data reported in this paper is 2.4 μm , providing overlap and a scaling interval with the Bell et al. (1985) data. We then scaled the entire spectrum to a geometric albedo 0.08 at wavelength 0.55 μm (see Appendix 1) giving us the final geometric albedo plot from 0.3 to 3.8 μm (Figure 2).

3. ANALYSIS OF DARK SIDE SPECTRUM – PREVIOUS WORK

Having confirmed the existence of the strong 3 μm absorption and characterized it in more detail, we will begin our analysis by considering some of the specific proposals for individual components of the dark side material made by previous investigators.

3.1. HCN POLYMERS

We first consider the possible role of HCN-polymer. This substance was an essential component in all of the models judged acceptable by Wilson and Sagan (1996), because it provided the steep red slope of the dark side spectrum observed at visible wavelengths.   This red slope is illustrated in Figure 3, which compares the albedo of the dark side with asteroids of classes C, P and D, from 0.45 – 2.3 μm . As other authors have noted, the dark side of Iapetus has a higher reflectivity at these wavelengths (it is redder) than any of these asteroids (Vilas and Smith 1985; Bell et al. 1985). Yet the red slope is not as steep as that of the Centaur 5145 Pholus (Fink et al. 1992).

FIGURE 3

Our observations do not extend to the 4 to 5 μm region singled out by these authors as offering the opportunity for a definitive identification of HCN polymer from the - C $\equiv$ N vibration fundamental near 4.6 μm . But we do cover the 3.0 – 3.8 μm region, where this compound contributes a broad absorption to the spectrum.

The presence of the well-known ice absorptions at 1.5 and 2.0 μm in our composite spectrum (Figure 2) signal that the deep absorption at 3 μm must contain a significant contribution from water ice. We attempted to fit this band with the "best-fit"

model parameters of Wilson and Sagan (1995) (7.9 μm grains consisting of 30% poly HCN, 55% H_2O ice, and 15% bulk Murchison meteorite) using approximately the same mixing method they employed – a linear combination of optical constants (Appendix 2). We agree with the Wilson-Sagan model to within ± 10% over the same range of wavelengths they considered (0.3 – 2.5 μm), but this combination of surface materials fails to reproduce the shape of the 3.0 μm feature, as anticipated from simple inspection of the wavelength dependence of the optical constants (Figure 4 of Wilson and Sagan 1995). With 30% poly HCN in the mixture, the resulting spectrum is too dark at 3.5 μm by nearly a factor of 2 compared with our observations (Figure 4). We conclude that:

FIGURE 4

A.   Poly HCN cannot be the reddening agent in the Iapetus dark material, because it would contribute too much absorption from 3.0 to 3.8 μm.   While some smaller amount of poly HCN may be present, there is *no reason to include it.* Some other substance that has a steep red slope in visible light but does not absorb at 3.5 μm would provide a better spectral analogue.

3.2. HYDRATED SILICATES

This component was originally introduced by Veeder and Matson (1980) to explain broad band 1.6 μm and 2.2 μm photometry of the dark side of Iapetus and was subsequently invoked by Lebofsky et al. (1982) as a contributor to the strong 3.0 μm absorption. However, the latter authors noted that they had to add water frost to their areal mixture of water ice at the dark side poles (~ 10% of projected area) and the Murchison bulk material they used to make up the dark coating, in order to achieve sufficient depth of the 3.0 μm feature. Vilas et al. (1996) also attributed the 3.0 μm feature to hydrated silicates, which they thought would include the aqueously altered iron minerals they proposed (see below). In retrospect, the original invocation of this component appears to stem from the attribution of the low 3 μm albedo of 1 Ceres to the presence of hydrated silicates on that dark, G-type asteroid (Lebofsky 1978). Subsequent observations have documented the presence of hydrated silicates on most C-class

asteroids, while the outermost P- and D-class asteroids appear to be anhydrous (Scott et al. 1989). Wilson and Sagan (1995, 1996) emphasized that they did not need hydrated silicates to obtain their best fits to the 0.3 – 2.5 μm spectrum of Bell et al. (1985), and we find that this conclusion applies to the 2.8 – 3.8 μm region as well.

Inspection of Figure 1 reveals a small relative maximum at ~3.1 μm in the strong absorption occurring in both the bright and dark side Iapetus spectra. We suggest that this feature represents selective (Fresnel) reflection from the surfaces of ice grains at the wavelength maximum of the H_2O-ice absorption. The relative maximum is present in spectra of Saturn's rings (Puetter and Russell 1977) and the iciest regions of Europa and Callisto (McCord et al. 1999, 2000). It is absent from spectra of ice-free regions on Callisto, where the presence of hydrated silicates has been invoked (e.g., Roush et al. 1990; Calvin et al. 1995; McCord et al. 1999).

In fact, the relative maximum at 3.1 μm is not present in spectra of hydrated silicates. This is illustrated in Figure 5, which shows the laboratory spectra of water ice, hydrated silicates, and their intimate mixtures. All of these data were obtained with sample temperatures near 80 K (Roush et al. 1990). Spectra of both coarse and fine-grained water ice exhibit a reflectance peak near 3.12 μm whereas spectra of montmorillonite and a palagonite do not. When these two components are mixed with water ice at the level of 5 % by weight, the Fresnel peak is only weakly influenced, but at 10 wt.% contaminants the Fresnel peak is virtually eliminated. This illustrates that only modest amounts of contaminants are required to subdue the presence of the Fresnel peak. Hence, we conclude that:

FIGURE 5

B.   While some hydrated silicates may be present on the dark side of Iapetus, e.g., in isolated patches, there is *no feature in the spectrum that requires their existence.*

3.3. IRON-BEARING MINERALS

Vilas et al. (1996) removed a straight line continuum to illustrate more clearly the 0.67 micrometer band in their Iapetus data. They defined the continuum by fitting a

straight line through their data points from approximately 0.48 – 0.88 μm. In order to provide a comparison of the spectra of iron oxides/oxyhydroxides and ferrous sulfates (e.g., Clark et al. 1993) to the Iapetus spectrum we have reverted to a simple comparison of laboratory and Iapetus spectra. The results are shown in Figure 6 for the 0.35 – 2.5 μm wavelength region. We have attempted to include the range of spectral variation exhibited by the laboratory spectra by reproducing two spectra for each laboratory sample.

FIGURE 6

As Vilas et al. (1996) point out, if their identification of the 0.67 μm absorption in the spectrum of Iapetus is correct, a much stronger absorption should be present between 0.75 μm and 0.95 μm , arising from the $^6A_1 \rightarrow {}^4T_2$ (G) Fe^{3+} transition that involves the same ground state (Adams 1975; Hunt and Ashley 1979). Inspection of Figure 6 shows no evidence of this feature. We have looked without success for other indications of iron minerals at longer wavelengths. We conclude that:

C. There is no *consistent* evidence for the presence of iron minerals in the dark material in Iapetus. The structure in the redward slope of the visible spectrum described by Vilas et al. (1996), including the 0.67 μm absorption, invites additional observations. that should be extended to 1.00 μm. The 0.67 μm feature may be the result of an as yet unidentified absorber

4. ANALYSIS OF THE DARK SIDE SPECTRUM – A NEW PERSPECTIVE

Having said what is *not* indicated by the new spectral data presented here, we now attempt to interpret these results with our own models. The keen edge of Occam's razor urges us to use the minimum number of components that will provide a fit to the spectrum, with each component being as simple and well-defined as possible. In practice, we have found that we can fit the entire 0.3 – 3.8 μm spectrum of the leading hemisphere (excluding the 0.67 μm feature) with just three components: water ice, a

dark, spectroscopically neutral component (we use amorphous carbon), and a reddish, nitrogen-rich compound with very specific properties in the 2.8 – 3.8 μm region (we use Triton tholin, Khare et al. 1994b) .

We arrived at this mixture by trying to satisfy the following observational constraints:

1. The low albedo.
2. The red slope from 0.3 – 1.5 μm .
3. The shapes and depths of the ice absorptions at 1.5 and 2.0 μm .
4. The shape and depth of the 3.0 μm absorption.

4.1 CARBON AND WATER ICE

Amorphous carbon nicely accounts for the first observational constraint. It is a stand-in for any suitably dark substance that is spectrally neutral over the observed wavelength range. Note that this neutrality means that carbon alone cannot satisfy the other constraints.

Amorphous or poorly graphitized carbon is the most abundant carbon-rich material in interplanetary dust particles (IDP's) (Thomas et al. 1993; Keller et al. 1994). Carbon particles are also found in the interstellar medium (for reviews see van Dishoeck et al. 1993, and Whittet and Tielens 1997). Carbon grains were identified as carrying 8 to 10% of the total solid carbon in Halley's comet (Fomenkova 1997). Electron, ion, and UV irradiation of hydrocarbon compounds at low temperatures also produces a "carbonization" of this material that darkens and reddens it in the process (e.g., Thompson et al. 1987, Strazzulla 1997, Allamandola et al. 1988). We do not have optical constants for all of these materials so we are forced to restrict our neutral, dark component to amorphous carbon.

There is no doubt that the component principally responsible for the 3.0 μm absorption (constraint No. 4) is water ice. This is demonstrated in Figure 7, which shows model spectra computed for varying proportions of ice and amorphous carbon. With sufficient ice to match the well-known 1.5 and 2.0 μm features (constraint No. 3), the models produce an absorption at 3 μm whose depth matches that of the feature in the dark side spectrum. However, if ice and carbon are the only components, they produce a

13

feature that is much too broad, with too much absorption at 3.3 μm, and which gives an albedo in the 0.3 – 1.5 μm region that is too high (Figure 7). Increasing the grain size of the ice incrementally from 6.3 to 150 μm makes the fit for $\lambda > 3.3$ μm even worse. We have therefore maintained the 6.3 μm grain size, which is close to the smallest value compatible with the Hapke theory at these wavelengths. (A grain size closer to the wavelength would violate the boundary conditions of the theory.)

FIGURE 7

4.2 ORGANIC COMPOUNDS

We need an additional component that is more reflective than ice from 3.3 – 3.5 μm . It would obviously be helpful if this same component could produce the observed red slope in the visible light spectrum (constraint No. 2). Silicates and organics are both possible candidates, but as silicates are not sufficiently red (Fig. 7), we have turned to organic compounds. Some organic compounds in IDPs survive atmospheric entry to Earth, and we similarly expect some organic material to survive emplacement (or exposure) on Iapetus. Here there is a huge variety of compounds to work with, but the interplay between constraints (2) and (4) rapidly narrows the field. For example, we have seen that while poly HCN can satisfy (2), it fails with (4).

To find an alternative to poly HCN, we seek an organic compound that is likely to be present and whose optical properties have been determined. This is a major limitation on any effort to match an astronomical spectrum with one or more organic compounds: As in the case of carbon, our investigation of alternatives is unfortunately limited to substances for which the optical constants are known (Table 2). Among these substances are various extracts from carbonaceous meteorites and several so-called "tholins", the solid products of coronal discharges through mixtures of different gases. We have examined Titan tholin, made from a 90:10 mixture of $N_2:CH_4$ gases – simulating the present atmosphere of Titan (Thompson et al. 1991), Triton Tholin, from a 99.9:0.1 mixture of $N_2:CH_4$ gases – simulating the present atmosphere of Triton (Thompson et al. 1989), and ice tholin, produced by charged particle irradiation of a 1:6 mixture of solid $C_2H_6:H_2O$ at 77 K (Khare et al. 1993). We have also considered a

kerogen, which is a waxy complex organic material, biologically derived, that is found in terrestrial sediments (Khare et al. 1990). Kerogen-like solids are found in meteorites and there has been an astronomical tradition to use kerogens as a "stand-in" for the dark, reddish presumably organic materials found on dark objects in the outer solar system (Khare et al. 1990). However, meteoriticists prefer the term macromolecular carbon to refer to the insoluble organic residue that is left after prolonged treatment of carbonaceous chondrites with various solvents, including acids (Cronin et al. 1988). Given its biological origin, kerogen is obviously not a realistic substitute for meteoritic material, so we have also examined the Murchison extract previously referred to in section 3.1.

TABLE 2

We found that of these five organic compounds, only Triton tholin provides the necessary reflectivity at 3.4 μm to counteract the deep absorption of amorphous carbon and H_2O ice and satisfy constraint No. 4. The reason for this success lies with the elemental composition of Triton tholin, which exhibits a ratio of nitrogen to carbon N/C = 1.33, compared with 0.67 in Titan tholin (McDonald et al. 1994). For comparison, it is useful to note that the solar value of N/C = 0.33 (Anders and Grevesse 1989) while in C1 carbonaceous chondrites, N/C = 0.1 (Vdovykin and Moore, 1975; Moore 1975), and in comets N/C = 0.05 (Geiss 1988). In the macromolecular carbon compounds in carbonaceous chondrites N/C < 0.03 (Cronin et al. 1988). Of 123 molecules found so far in the gas phase in interstellar clouds (L. E. Snyder, private communication) only one, NH_2CH, contains more N than C. Evidently, this surplus of nitrogen is rare in non-biological organic compounds, whereas it is not uncommon in terrestrial biochemistry (N/C = 2 in urea, for example). The high N/C ratio produces marked effects on the spectrum of Triton tholin.

The near-IR spectrum of Titan tholin contains a strong, broad, double-peaked absorption with maxima at 3.02 and 3.13 μm. These two bands were interpreted by McDonald et al. (1994) as N-H stretching features, probably arising from amino (NH_2) groups. The near-IR spectrum of Triton tholin is clearly different. A single, intense

absorption occurs at 2.92 μm, and this is again assigned to the N-H stretching vibration (McDonald et al. 1994), but in this case, it may be caused by – NH rather than - NH$_2$ (Colthup et al. 1975). These characteristics of the Triton tholin absorption provide the complementary features we need: adding Triton tholin to ice steepens the longward side of the H$_2$O ice absorption at 3.5 μm, matching the feature observed in the spectrum of Iapetus, while Titan tholin produces too much absorption at 3.2 – 3.7 μm (Figure 8).

FIGURE 8

Unfortunately, the interpretation of the near IR laboratory spectra of these compounds is not sufficiently precise to enable us to identify the key differences in composition that lead to this result. Clearly it is the weakness of the 3.13 μm feature in the Triton tholin that produces the proper fit, and this appears to be the result of a difference in the relative importance of NH$_2$ and NH in determining the absorptions in this region. Ice tholin (Khare et al. 1993) has a strong, double-peaked absorption at 3.4 μm, which is caused by the C-H stretch in aliphatic compounds. This same feature appears in methane clathrate darkened by charged particle irradiation (Thompson et al. 1987). It is not present in the spectrum of Triton tholin and it does not occur in the dark side spectrum of Iapetus.

To summarize, the key spectral feature needed to satisfy constraint No. 4 is a sharply peaked absorption near 2.9 μm , with significantly decreasing absorption at longer wavelengths. This requires the presence of a specific N-H stretch that we have only found in the material called Triton tholin, which contains N/C > 1, a rare proportion in astronomical organic compounds. The C-H bond absorption near 3.4 μm is absent from the Iapetus spectrum, thereby ruling out a host of dark, reddish organic compounds. Finally, Triton tholin also produces the correct red slope at shorter wavelengths that is required to satisfy constraint No. 2.

Now we can introduce a fifth constraint to fine tune the models: the turning down of the albedo at 3.8 μm caused by ice absorption and the steep slope at 3.3 μm from the

Triton tholin allow us to adjust the relative abundances of ice and tholin in our mixture. The best fit using our three components is shown in Figure 9.

FIGURE 9

4.3 CONTRIBUTIONS FROM THE ICY POLES

All of the models we have described so far represent intimate mixtures, in which the particles of the different materials are adjacent to one another and an incoming solar photon interacts with all the materials before being scattered out of the surface. However, there is some segregated bright material contributing to the spectrum illustrated in Figure 2. The observations of the dark side of Iapetus – even when obtained at maximum eastern elongation – always include a contribution of bright side material at the satellite's poles. Lebofsky et al. (1982) estimated that the bright poles contributed about 10% of the total light producing their dark side spectrum.

To account for the spatial separation of dark and light material contributing to the spectrum illustrated in Figure 2, we developed a few models using spatial mixtures of our selected components. Suppose the ice absorption in our spectrum is actually contributed by the polar caps, not by ice mixed with dark material. To test this possibility, we tried combining an intimate mixture of Triton tholin and amorphous carbon with spatially separated, pure H_2O ice. The resulting models fail to fit both the weaker 1.5 and 2.0 μm features and the 3.0 μm absorption to differing degrees, depending on the proportions. For example, as shown in Figure 10, when 30% H_2O ice is spatially mixed with the intimate mixture of Triton tholin and amorphous carbon, the model feature at 3 μm is too triangular in shape, the overall geometric albedo is too high, and the weaker H_2O features are too strong. Decreasing the H_2O component improves the fit for the weaker features but still fails to match the 3 μm absorption and produces a geometric albedo that is too low at $\lambda \leq 2.5 \mu m$.

FIGURE 10

We then attempted to fit models in which all three components were spatially segregated from one another. Three of these models are shown in Figure 11. Once again, it is impossible to fit the reddending in the visible, the strengths of the three ice bands and the albedo at 2.5 μm simultaneously.

FIGURE 11

This exercise substantiates the conclusion of Lebofsky et al. (1982) that *the 3 μm feature is produced by the dark side material*, it is not the result of a contribution from bright side ice at the satellite's poles. To achieve a good fit at 3 μm, it is necessary to add H_2O ice to the intimate mixture of carbon and Triton tholin, in the proportions originally deduced. We can then accommodate ~2 percent of pure H_2O ice at the poles, as shown in Figure 12.

FIGURE 12

This analysis also demonstrates that Bell et al. (1985) overcompensated in their removal of all traces of ice absorption from this spectrum. In fact, the intimate mixture that we have found as the best match to the 0.3 − 3.8 μm spectrum contains enough ice to fit the absorptions at 1.5 and 2.0 μm (Figure 9).

5. CONCLUSIONS

While we have successfully matched a span from 0.3 to 3.8 μm of the low-albedo hemisphere spectrum with an intimate mixture of only three components, we cannot claim to have a unique fit. As always in such endeavors, we thirst for more wavelengths and more optical constants. Our first project is to complete the "L" window spectrum, recording 3.8 - 4.15 μm. This will provide further finesse for balancing the effects of Triton tholin against those of ice in our model spectrum. The data we have are inconclusive on this point, indicating a steeper slope just beyond 3.6 μm than the model provides (Figure 13).

FIGURE 13

The next step is to explore the 5 μm window, which offers a new discriminant. The laboratory spectrum of Triton tholin shows no evidence of the -C≡N absorption near 4.6 μm associated with nitriles (-C≡N) or isonitriles (-N≡C) (Bernstein et al. 1997), whereas HCN polymer and Titan tholin both do (McDonald et al. 1994; Cruikshank et al. 1991; Khare et al. 1994). The absence of this feature in the Iapetus spectrum would strengthen the case for an organic compound that is highly enriched in nitrogen, because if the 3.0 μm band is due to an N-H component and the C-N component at 4.6 μm is absent, then the ratio of N/C is greater. Both tholins exhibit strong absorptions beginning at 6 μm, which again are very different. Titan tholin produces two absorption maxima at 1650 cm^{-1} (6.06 μm) and 1560 cm^{-1} (6.41 μm), probably caused by the C = C vibration, whereas Triton tholin has a single feature at 1636 (6.11 μm) cm^{-1} (McDonald et al. 1994). Observations of these wavelengths are not possible from Earth, but they fall within the range of the CIRS instrument on the Cassini orbiter. This region of the spectrum will also allow a search for products from the irradiation of CO_2 and H_2O (Moore et al. 1991; Strazzulla 1997). The VIMS instrument on Cassini will fill in the gaps at 2.7 μm and 4.3 μm in Earth based spectra, allowing a search for the strong CO_2 bands that occur in these two intervals. In Figure 12 we show the differences between our model and the Wilson-Sagan (1996) model in the 3-5 μm range, which VIMS will be able to record. Evidently we can expect considerable additional insight into the nature of the Iapetus dark material when the Cassini Mission reaches Saturn in 2004.

Meanwhile, it is important to return to the visible spectrum with higher resolution and signal precision to investigate the 0.67 μm feature discovered by Vilas et al. (1996) as well as the other structures these authors reported in this part of the spectrum. We need this study not only for Iapetus, but also for Hyperion and Phoebe (see Jarvis et al. 2000), to continue the exploration of possible linkages among these satellites.

What did cause this dark material to appear on Iapetus, and does it occur on other objects? What is its source, and how did it obtain such a high proportion of nitrogen? We can pursue these questions by investigating the 2.85 – 4.15 μm spectrum of other

dark objects, to see how similar their spectra are to Figure 2. We can already report that there is no evidence of Iapetus dark material in the rings of Saturn (Puetter and Russell 1977), on the surfaces of the Galilean satellites of Jupiter (McCord et al. 1999), or on 624 Hektor, the largest Trojan asteroid (Cruikshank et al., in preparation). We also know that the red slope of the visible spectrum of the Iapetus dark side sets it apart from all except the reddest D asteroids (Figure 3). It is significantly different from the reflectivity of the surface of Phoebe, which has a flatter spectrum in the visible (Tholen and Zellner 1983). Hyperion, however, circling Saturn just inside the orbit of Iapetus, exhibits a similar reddish slope at short wavelengths, although its ice absorptions are more pronounced in the $1 - 2.5 \mu m$ region (Tholen and Zellner 1983; Cruikshank et al., in preparation). Perhaps Hyperion has a thinner coating of the dark material that is present on the leading hemisphere of Iapetus (Matthews 1992; Banaszkiewicz and Kirov 1997). We need to record the $2.85 - 4.15 \mu m$ region of this satellite's spectrum to know. We do support the idea that the dark material is a coating rather than a lag deposit produced by abrasion and evaporation of surface ice. This latter process would surely come into play with the formation of impact craters on Iapetus, and there are no reports of dark ejecta blankets in the bright hemisphere (Squyres et al. 1984; Buratti and Mosher 1995).

We close with a somewhat daring hypothesis that we think is worthy of Eddington's Icarus (see frontispiece, this issue). We point out that Iapetus happens to be quite near an object that has been producing dark, nitrogen-rich organic material through atmospheric photochemistry for 4.5 GY, viz Titan. While today CH_4 constitutes a few percent of Titan's atmosphere, the discovery that Titan's nitrogen is highly fractionated (Marten et al. 1997; Meier et al. 1997) suggests that early epochs may well have included times of ~0.1% CH_4, especially in the photochemically vulnerable stratosphere. The key point here is that we need an environment with $N_2/CH_4 \gg$ Solar N/C to produce the organic material that fits constraints (2) and (4). A nitrogen-rich atmosphere is certainly an obvious candidate for such an environment. (Are there others?) Could an impact on Titan spray a surface layer of accumulated organic aerosols into trans-Saturnian space, there to be swept up by Hyperion and Iapetus? Could Hyperion itself be a relic of this impact event? If such a catastrophe really happened, we would expect some of this dark material to move inward from Titan as well, where it should now underlie the icy frost on

the inner satellites, covered by ice particles continually accreted from the E-ring. Perhaps we see signs of this dark material in the surprisingly low short wavelength albedos of these objects (Cruikshank et al., in preparation).

What a violent history the Saturn system seems to show us! Icy fragments abound in the form of "Trojan" satellites and ring moons. The low densities of Mimas and Enceladus suggest that these objects may also be daughters of one or more collisions. Clearly the Cassini mission will make many new discoveries in this fascinating place!

APPENDIX I

NOTE ON THE SCALING TO ALBEDO 0.08 AT 0.55 μm:

The disk-averaged geometric albedo, p_V of the leading hemisphere of Iapetus (seen from Earth at the satellite's eastern elongation) can be calculated from the brightness at 0.55 μm (the V photometric band), expressed in stellar magnitudes, and denoted by V, from

$$V = V_0 - 2.5 \log p_V - 5 \log r + 5 \log (R\,D)$$

Where V_0 is the magnitude of the Sun (taken as -26.75), r is the satellite's radius (720 km, or 4.813×10^{-6} AU), R and D are the heliocentric and geocentric distances (in AU), respectively. A correction for the solar phase angle (alpha) of 0.039 mag/degree can be applied to correct the V magnitude to zero phase angle; this factor has been derived for asteroids of low albedo in the absence of a strong opposition brightness surge.

The V magnitude of Iapetus for 4 March 1979 at 1100 UT, just 4.4 hours before maximum eastern elongation, was given by Cruikshank et al. (1983) as 12.02 ($\pm$ 0.005) at R = 9.329 AU, D = 8.339 AU, and alpha = 0.34 $^\circ$, from which $p_V = 0.083$ (+ 0.008 – 0.004). We have adopted $p_V = 0.08$, similar to the value derived by Squyres et al. (1984).

APPENDIX II

DUPLICATING THE WILSON-SAGAN (1995) MODEL SPECTRUM

We have calculated the Wilson and Sagan model using the sum of the optical constants that they show (heavy line in their Figure 4), but the resulting spectrum does not fit the data in the way that they show in their Figure 2. To produce this spectrum, we relied on Hapke's (1993 and references therein) treatment of the interaction of light with particulate matter on the surfaces of solid bodies, following the procedures reviewed by Roush (1994) and by Cruikshank et al. (1998b). Typical input parameters for each

22

component in a mixture include the optical constants, grain size, and relative abundances. The optical constants for the materials used in this study are cited in Table II.

We then found that we could approximate the Wilson-Sagan model by making certain *ad hoc* adjustments to their combination of the optical constants of their components, followed by normalization to geometric albedo 0.08 at 0.55 μm , and this is the model spectrum we show in Figures 4 and 12 of the present paper. As this spectrum matches the observations out to 2.5 μm very well, we believe that the differences between their published model curve and our recomputation of it arise from uncertainties in the way in which the component optical constants were combined by the original authors, rather than from gross differences in the model computational technique. We note that Cruikshank et al. (1998a) reproduced the Wilson et al. (1994) model of 5145 Pholus using the same Hapke modeling code as used in the present paper, thus suggesting that some factor other than the precise details of the code is causing the discrepancy in the recomputation of the Wilson and Sagan Iapetus model.

ACKNOWLEDGEMENTS

REFERENCES

Adams, J. B. 1975. Interpretation of visible and near-infrared diffuse reflectance spectra of pyroxenes and other rock forming minerals. In *Infrared and Raman Spectroscopy of Lunar and Terrestrial Minerals* (C. Karr, Jr., Ed.), pp. 91-116, Academic Press, New York.

Allamandola, L. J., S. A. Sandford, and G. J. Valero 1988. Photochemical and thermal evolution of interstellar/precometary ice analogs. *Icarus* **76**, 225-252.

Anders, E., and N. Grevesse 1989. Abundances of the Elements: Meteoritic and Solar. *Geochim. et. Cosmochim. Acta.* **53**, 197-214.

Banaszkiewicz, M. and A. V. Kirov 1997. Hyperion as a dust source in the Saturnian system. *Icarus* **129**, 289-303.

Barucci, M. A., M. Lazzarin, T. Owen, C. Barbieri, and M. Fulchignoni 1994. Near-infrared spectroscopy of dark asteroids. *Icarus* **110**, 287-291.

Bell, J. F., D. P. Cruikshank, and M. J. Gaffey 1985. The composition and origin of the Iapetus dark material. *Icarus* **61**, 192-207.

Bernstein, M. P., S. A. Sandford, and L. J. Allamandola 1997. The infrared spectra of nitriles and related compounds frozen in Ar and H_2O. *Astrophys J.* **476**, 932-942.

Buratti, B. J., and J. A. Mosher 1995. The dark side of Iapetus: Additional evidence for an exogenous origin. *Icarus* **115**, 219-227.

Calvin, W. M., Clark, R. N., Brown, R. H. and Spencer, J. R. 1995. Spectra of the icy Galilean satellites from 0.2 to 5 µm: A compilation, new observations, and a recent summary. *J. Geophys. Res.* **100**, 19041-19048.

Cassini, J. D. 1673. A Discovery of two new planets about Saturn, made in the Royal Parisian Observatory by Signor Cassini. *Philos. Trans. R. Soc.*, **8**, 5178-5185.

Clark, R. N., G. A. Swayze, A. J. Gallagher, T. V. V. King, and W. M. Calvin. 1993. The U.S. Geological Survey Digital Spectral Library, Version 1: 0.2 to 3.0 µm , USGS Open Report 93-592, 1340 pages. http://speclab.cr.usgs.gov

Colthup, N. B., L. H. Daly, and S. E. Wiberly 1975. *Introduction to Infrared and Raman Spectroscopy.* Academic Press, New York.

Cook, A. F., and F. A. Franklin 1970. An explanation of the light curve of Iapetus. *Icarus* **13**, 282-291.

Cronin, J. R., S. Pizzarello, and D. P. Cruikshank 1988. Organic matter in carbonaceous chondrites, planetary satellites, asteroids and comets. In *Meteorites and the Early Solar System* (J. F. Kerridge and M. S. Matthews, Eds.), pp 819-857, Univ. of Arizona Press, Tucson.

Cruikshank, D. P., L. J. Allamandola, W. K. Hartmann, D. J Tholen, R. H. Brown, C. N. Matthews, and J. F. Bell 1991. Solid C ≡ N bearing material on outer solar system bodies. *Icarus* **94**, 345-352.

Cruikshank, D. P., J. F. Bell, M. J. Gaffey, R. H. Brown, R. Howell, C. Beerman, and M. Rognstad 1983. The dark side of Iapetus. *Icarus* **53**, 90-114.

Cruikshank, D. P., T. L. Roush, M. J. Bartholomew, T. R. Geballe, Y. J. Pendleton, S. M. White, J. F. Bell, III, J. K. Davies, T. C. Owen, C. de Bergh, D. J. Tholen, M. P. Bernstein, R. H. Brown, K. A., Tryka, and C. M. Dalle Ore. 1998a. The Composition of Centaur 5145 Pholus. *Icarus* **135**, 389-407.

Cruikshank, D. P., T. L. Roush, T. C. Owen, E. Quirico, and C. de Bergh 1998b. The surface compositions of Triton, Pluto, and Charon. In *Solar System Ices* (B. Schmitt, C. de Bergh, and M. Festou, Eds.), pp. 655-684, Kluwer Academic Pub., Dordrecht.

Dumas, C., T. Owen and M. A. Barucci 1998. Near-Infrared Spectroscopy of Low-Albedo Surfaces of the Solar System: Search for the Spectral Signature of Dark Material. *Icarus* **133**, 221-232.

Fink, U., M. Hoffman,n., W. Grundy, M. Hicks, and W. Sears 1992. The steep red spectrum of 1992 AD: An asteroid covered with organic material? *Icarus* **97**, 145-149.

Fomenkova, M. N. 1997. Organic components of cometary dust. In *From Stardust to Planetesimals*, (Y. J. Pendleton and A. G. G. M. Tielens, Eds), ASP Conference Series, ASP, Provo, **122**, 415-422.

Geiss, J. 1988. Composition of Halley's comet: Clues to origin and history of cometary matter. *Rev. Mod. Astron.* **1**, 1-27.

Hamilton, D. P. 1997. Iapetus: 4.5 billion years of contamination by Phoebe dust. *Bull. Am. Astron. Soc.* **29**, 1010 (Abstract).

Hansen, G. B., and McCord, T. B. 2000. Amorphous and crystalline ice on the Galilean satellites: A balance between thermal and radiolytic processes. Lunar and Planetary Science Symposium XXX1, Abstract 1630.

Hapke, B. W. 1993. *Theory of Reflectance and Emittance Spectroscopy*, Cambridge Univ. Press, New York.

Hudgins, D. M., S. A. Sandford, L. J. Allamandola, and A. G. G. M. Tielens. 1993 Mid- and far-infrared spectroscopy of ices: Optical constants and integrated absorbances. *Astrophys. J. Supp.* **86**, 713-870.

Hunt, G. R., and Ashley, R. P. 1979. Spectra of altered rocks in the visible and near-infrared. *Econ. Geol.* **74**, 1613-1628.

Jarvis, K. S., F. Vilas, S. M. Larson, and M. J. Gaffey 2000. Are Hyperion and Phoebe linked to Iapetus? *Icarus* (in press).

Keller, L. P., K. L. Thomas, and D. S. McKay 1994. Carbon in primitive interplanetary dust particles. In *Analysis of Interplanetary Dust* (M. E. Zolensky, T. L. Wilson, F. J. M. Rietmeijer, and G. J. Flynn, Eds.), pp. 159-164, AIP Conference Procedings **310**, Amer. Inst. Phys, New York.

Khare, B., C. Sagan, W. R. Thompson, E. T. Arakawa, C. Meisse, and P S. Tuminello. 1994a. Optical properties of poly-HCN for astronomical applications. *Can. J. Chem.* **72**, 678-694.

Khare, B. N., C. Sagan, M. Heinrich, W. R. Thompson, E. T. Arakawa, P. S. Tuminello, and M. Clark. 1994b. Optical constants of Triton tholin: Preliminary results. *Bull. Am. Astron. Soc.*, **26**, 1176-1177 (abstract).

Khare, B. N., W. R. Thompson, C. Sagan, E. T. Arakawa, C. Meisse, and I. Gilmour. 1990. Optical constants of kerogen from 0.15 to 40 μm: Comparison with meteoritic organics. In First Inst. Conf. On Lab. Res. For Planetary Atmospheres, NASA CP-3077, 340-356, NASA, Washington, D.C.

Khare, B. N., W. R. Thompson, L. Cheng, C. F. Chyba, C. Sagan, E. T. Arakawa, C. Meisse, and P. S. Tuminello 1993. Production and optical constants of ice tholin

from charged particle irradiation of (1:6) C_2H_6 / H_2O at 77 K. *Icarus* **103**, 290-300.

Lebofsky, L. A. 1978. Asteroid 1 Ceres: Evidence for water hydration. *Mon. No. Roy. Astron. Soc* **182**, 17P-21P.

Lebofsky, L. A., M. A. Feierberg and A. T. Tokunaga 1982. Infrared observations of the dark side of Iapetus. *Icarus* **49**, 382-386.

Luu, J., D. Jewitt and E. Cloutis 1994. Near-Infrared Spectroscopy of Primitive Solar System Objects. *Icarus* **109**, 133-144.

Marten, A., T. Hidayat, R. Moreno, G. Paubert, B. Bézard, D. Gautier, T. and Owen, T. 1997. Saturn VI (Titan), *IAU Circular 6702*, 19 July.

Matthews, R. A. J. 1992. The darkening of Iapetus and the origin of Hyperion. *Q. J. Roy. Astron. Soc.* **33**, 253-258.

McCord, T., and 11 co-authors. 1999. Hydrated salt minerals on Europa's surface from the Galileo near-infrared mapping spectrometer (NIMS) investigation. *J. Geophys. Res.* **104**, 11827-11851.

McDonald, G. D., W. R. Thompson, M. Heinrich, B. N. Khare, and C. Sagan. 1994. Chemical investigation of Titan and Triton tholins. *Icarus* **108**, 137-145.

Meier, R., T. Owen, H. E. Matthews, A. Marten, A., and D. Gautier 1997. Unpublished JCMT observations.

Moore, C. B. 1975. Nitrogen. In *Handbook of elemental abundances in meteorites* (B. Mason, Ed.) pp. 93-98, Gordon and Breach, New York.

Moore, M. H., R. Khanna, and B. Donn 1991. Studies of proton irradiated H_2O + CO_2 and H_2O + CO ices and analysis of synthesized molecules. *J. Geophys. Res.* **96**, 17541-17546.

Morrison, D., T. J. Jones, D. P. Cruikshank, and R. E. Murphy 1975. The two faces of Iapetus. *Icarus* **24**, 157-171.

Owen, T., D. Cruikshank, C. de Bergh and T. Geballe 1995. Dark matter in the outer solar system. *Adv. Space Res.* **16**, (2) 41-(2) 49.

Pendleton, Y. J., A. G. G. M. Tielens, A. T. Tokunaga, and M. P. Bernstein 1999. The interstellar 4.62 micron band. *Astrophys. J.* **513**, 294-304.

Puetter, R. C., and R. W. Russell 1977. The 2-4 μm spectrum of Saturn's Rings. *Icarus* **32**, 37-40.

Rouleau, F., and P. G. Martin 1991. Shape and clustering effects on the optical properties of amorphous carbon. *Astrophys. J.* **377**, 526-540.

Roush, T. L. 1994. Charon: More than water ice? *Icarus* **108**, 243-254.

Roush, T. L. 1996. Near-IR (0.8 – 2.5 μm) optical constants of water ice at 100 K. *Lunar Planet. Sci. Conf. XXVII.* Lunar Planet Inst. Houston, TX 1107-1108.

Roush, T. L., J. B. Pollack, T. C. Witteborn, J. D. Bregman, and J. P. Simpson 1990. Ice and minerals on Callisto: A reassessment of the reflectance spectra. *Icarus* **86**, 355-382.

Scott, E. R. D., G. J. Taylor, H. E. Newsom, F. Herbert, M. Zolensky and J. F. Kerridge 1989. Chemical, thermal and impact processing of asteroids. In *Asteroids II* (R. P. Binzel, T. Gehrels and M. S. Matthews, Eds.) pp. 701-739. Univ. of Arizona Press, Tucson.

Soter, S. Brightness of Iapetus. A paper presented at IAU Colloquium 28, Cornell Univ., Ithaca, NY, 1983 (quoted by Wilson and Sagan 1995).

Squyres, S. W., B. Buratti, J. Veverka, and C. Sagan 1984. Voyager photometry of Iapetus. *Icarus* **59**, 426-435.

Strazzulla, G. 1997. Ion bombardment of comets. In *From Stardust to Planetesimals*, (Y. J. Pendleton and A. G. G. M. Tielens, Eds), ASP Conference Series, ASP, Provo, **122**, 423-434.

Tholen, D. J., and B. Zellner 1983. Eight-color photometry of Hyperion, Iapetus and Phoebe. *Icarus* **53**, 341-347.

Thomas, K. L., G. L. Banford, L. P. Keller, W. Klöck, and D. S. McKay 1993. Carbon abundance and silicate mineralogy of anhydrous interplanetary dust particles. *Geochim. et Cosmochim. Acta* **57**, 1551-1566.

Thompson, W. R., B. G. J. P. T. Murray, B. N. Khare, and C. Sagan 1987. Coloration and darkening of methane clathrate and other ices by charged particle irradiation: Applications to the outer solar system. *J. Geophys. Res.* **92**, 14,933 – 14,947.

Thompson, W. F., S. K. Singh, B. N. Khare, and C. Sagan 1989. Triton: Stratospheric molecules and organic sediments. *Geophys. Res. Lett.* **16**, 981-984.

Thompson, W. R., T. J. Henry, J. M. Schwartz, B. N. Khare, and C. Sagan 1991. Plasma discharge in N_2 + CH_4 at low pressures: Experimental results and applications to Titan. *Icarus* **90**, 57-73.

Van Dishoeck, E. F., G. A. Blake, B. T. Draine, and J. I. Lunine 1993. The chemical evolution of protostellar and protoplanetary matter. In *Protostars and Planets III* (eds. Levy, E. H. and Lunine, J. I., Eds.), pp. 163-241, Univ. Arizona Press, Tucson.

Vdovykin, G. P., and C. B. Moore 1975. Carbon. In *Handbook of elemental abundances in meteorites* (B. Mason, Ed.), pp. 81-92, Gordon and Breach, New York.

Veeder, G. J., and D. L. Matson 1980. The relative reflectance of Iapetus at 1.6 and 2.2 μm . *Astron. J.* **85**, 969-972.

Vilas, F., S. M. Larson, K. R. Stockstill and M. J. Gaffey 1996. Unraveling the zebra: Clues to the Iapetus dark material composition. *Icarus* **124**, 262-267.

Vilas, F. and Smith, B. A. 1985. Reflectance spectrophotometry (~0.5 – 1.0 μm) of outer-belt asteroids: Implications for primitive, organic solar system material. *Icarus* **64**, 503-516.

Warren, S. G. 1984. Optical constants of ice from the ultraviolet to the microwave. *Appl. Opt.* **23**, 1206-1225.

Whittet, D. C. B., and A. G. G. M. Tielens 1997. Infrared observations of interstellar dust absorption features. In *From Stardust to Planetesimals*, (Y. J. Pendleton and A. G. G. M. Tielens, Eds), ASP Conference Series, ASP, Provo, **122**, 161-178.

Wilson, P. D., and C. Sagan 1995. Spectrophotometry and organic matter on Iapetus. I. Composition models. *J. Geophys. Res.* **100** (E4), 7531-7537.

Wilson, P. D., and C. Sagan 1996. Spectrophotometry and organic matter on Iapetus 2. Models of interhemispheric asymmetry. *Icarus* **122**, 92-106.

Wilson, P. D., C. Sagan, and W. R. Thompson 1994. The organic surface of 5145 Pholus: Constraints set by scattering theory. *Icarus* **107**, 288-303.

TABLE 1 OBSERVING LOG

Date	UT	Wavelength Range (µm)	Integration Time (sec)	Sky Conditions	R (AU)	Δ (AU)	Orbital Position Angle θ	Hemi-sphere Visible	Air Mass
1997 Oct 6	0830-1000	3.18-3.82	3200	clear	9.395	8.399	76 deg	Leading	1.21-1.05
	1020-1035	2.40-3.05	384	clear				Leading	1.04
	1110-1210	2.78-3.42	2400	clear				Leading	1.05-1.17
	1250-1415	3.18-3.82	3840	clear				Leading	1.26-1.86
1998 Dec. 18	0510-0630	2.88-3.52	3360	thin cirrus	9.274	8.732	257 deg	Trailing	1.07-1.02
	0710-0840	3.48-4.12	3600	thin cirrus				Trailing	1.05-1.25

TABLE II. OPTICAL CONSTANTS USED IN MODEL CALCULATIONS

Component	Wavelength Range (μm)	Reference
Poly HCN	0.3-3.8	Khare et al. (1994a)
H_2O ice	0.3 - ~ 1.1, T ~ 230 K	Warren (1984)
	~ 1.1 – 2.5, T ~ 100 K	Roush (1996)
	2.5 – 3.8, T ~ 100 K	Hudgins et al. (1993)
Murchison Extract	0.3 – 2.5	Khare et al. (in preparation)
	2.5 – 3.8	Khare et al. (1990)
Triton Tholin	0.3 – 3.8	Khare et al. (1994b)
Amorphous Carbon		Rouleau and Martin (1991)
Kerogen		Khare et al. (1990)

FIGURE CAPTIONS

Figure 1. The new spectra of the dark, leading hemisphere (E) and the bright trailing hemisphere (W) of Iapetus in the 2.8 – 3.8 μm region. Note that the leading (E) hemisphere is actually brighter than the trailing (W) hemisphere in this wavelength region, yet its spectrum still shows characteristic features of the ice absorption that makes the trailing (W) hemisphere so dark at these wavelengths

Figure 2. The spectrum of the low-albedo hemisphere of Iapetus, 0.3 – 3.8 μm. This is a composite of the data obtained by Bell et al. (1985, Fig. 2) (triangles with errors bars), the data of Vilas et al. (1996) (continuous line, 0.3 – 0.9 μm), and the new data reported here (2.4 – 3.8 μm). Between 2.5 and 2.8 μm, where strong absorption occurs in the Earth's atmosphere, the spectrum is represented only by a few data points, connected here by a continuous smooth line. The point-to-point scatter in the data (2.4 – 3.8 μm) gives an indication of the probable errors in the individual data points. The composite spectrum has been scaled to geometric albedo 0.08 at 0.55 μm (See Appendix I).

Figure 3. A schematic representation of the spectral properties of low-albedo asteroids of the C, P, and D types (normalized to geometric albedo 0.05 at 0.55 μm) and those of the low-albedo hemisphere of Iapetus (normalized to geometric albedo 0.08 at 0.55 μm). The spectra of the asteroids exhibit a range of colors as indicated by the shaded region for each class. At visual wavelengths even the dark side of Iapetus is generally brighter than those asteroids, and it has a reddish color similar to the D-class asteroids.

Figure 4. The preferred model of the low-albedo hemisphere spectrum (dark material only) by Wilson and Sagan (1996), recalculated by us (as described in Appendix II) and compared to our new composite spectrum. The components used here in their Hapke scattering model are poly-HCN (an industrial HCN polymer), H_2O ice (from Warren 1984), and an acid-insoluble organic extract from the Murchison meteorite; the grain size of the composite material is 7.9 μm. Note that our composite spectrum exhibits more ice absorption, while Wilson and Sagan (1996) were matching the ice-free dark material spectrum produced by Bell et al. (1985). While the Wilson-Sagan model fits the spectrum below 2.5 μm quite well, it fails beyond 3.3 μm owing to the absorption of poly HCN in this region.

Figure 5. Reflectance spectra of granular samples of representative hydrated minerals palagonite (hydrothermally altered or weathered volcanic glass) and montmorillonite (a clay mineral), and water ice, all at temperatures relevant to the surface of Iapetus (~ 77 K). The top traces show water ice in both granulated (particles sizes < 90 μm) and large-particle (cm-size) form, with a magnified inset showing the region of the Fresnel reflection peak at about 3.12 μm. The second set of traces show the pure form of the minerals, while the inset shows granulated water ice (solid trace) and the absence of Fresnel peaks in the mineral spectral. The third and fourth traces show mixtures of water ice and the minerals in the proportions indicated. The effect of ≥ 10% mineral in an intimate mixture with H_2O ice is to suppress the Fresnel peak.

Figure 6. Laboratory spectra of iron oxides/oxyhydroxides (top two pairs of curves: hematite and goethite) and an iron-bearing sulfate (the pair of curves, second from bottom, jarosite) compared with the Iapetus data of Bell et al. (1985; points with errors), and Vilas et al. 1996, solid line). The insert at lower right is a magnified version of the boxed region of the Iapetus spectrum. The pairs (dotted and solid) of laboratory spectra illustrate the extremes of spectral behavior for each material. The vertical line at 0.67 μm corresponds to the wavelength where Vilas et al. (1996) identified a band in the Iapetus spectrum. The vertical line at 0.9 μm corresponds to the general region where an additional ferrous iron band should occur, as suggested by Vilas et al. (1996).

Figure 7. Model spectra for intimate mixtures of amorphous carbon with H_2O ice, both in grains of 6.3 μm size, compared with the spectrum of the low-albedo hemisphere of Iapetus. Note the poor fit from 3.1 to 3.6 μm, and the high reflectance at short wavelengths. The optical constants for H_2O ice at 100 K are from Hudgins et al. (1993).

Figure 8. A series of model spectra using an intimate mixture of H_2O ice (T = 100 K, as in Fig. 7), Titan tholin, and amorphous carbon; grain size 6.3 μm. Note the excess absorption in the models at 3.3 μm compared with the Iapetus data.

Figure 9. The best fitting model to the composite Iapetus spectrum consists of an intimate mixture of 25% H_2O ice (T = 100 K), 25% Triton tholin, and 50% amorphous carbon. The inset shows that the model (smooth line) fits the data of Bell et al. (1985) (open circles) and Vilas et al. (1996) (continuous line) about equally.
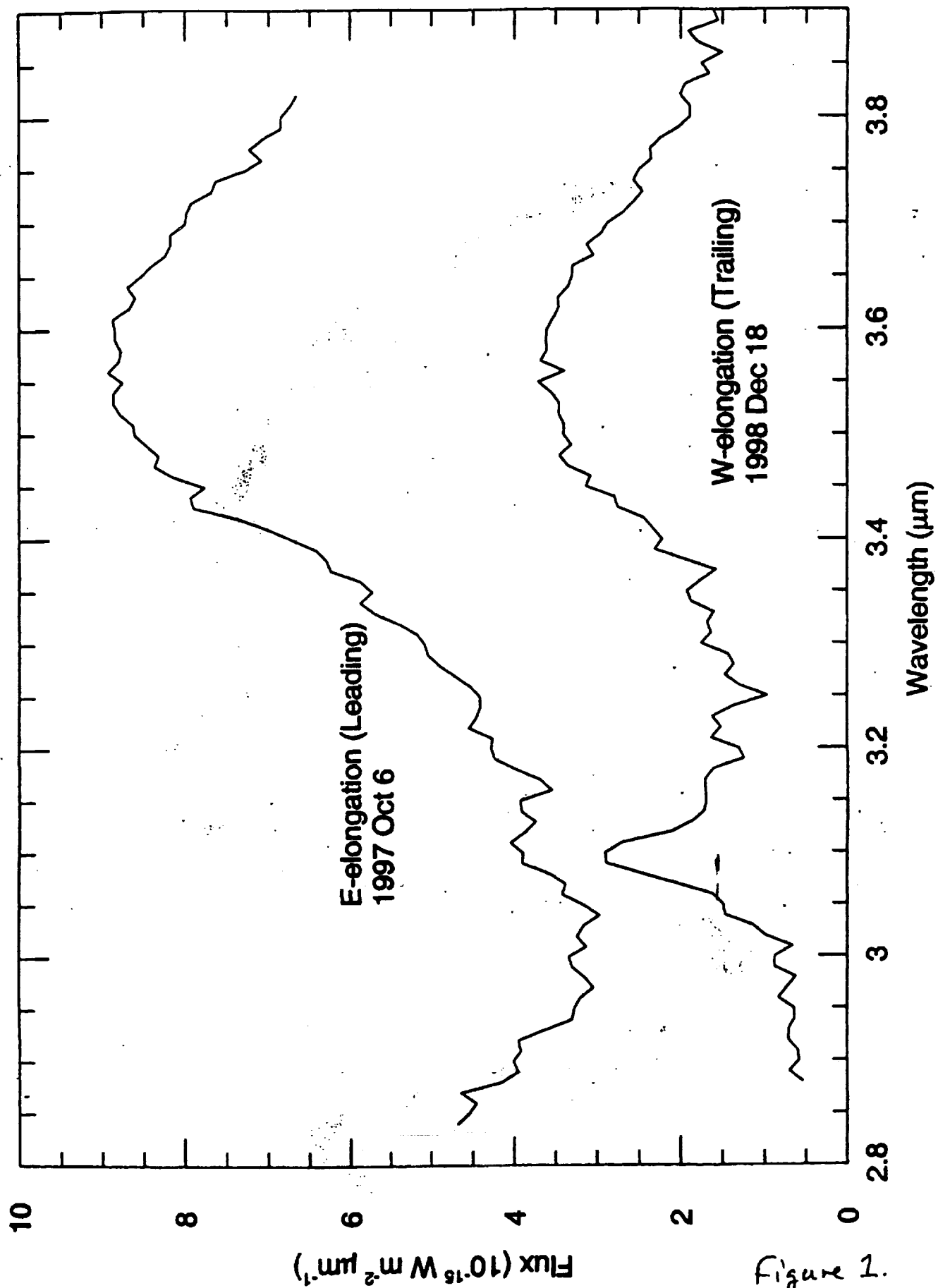
Figure 10. Spatially segregated models (area mixes) to test for the effects of isolated regions of H_2O ice on the low-albedo hemisphere of Iapetus. The Iapetus spectrum is shown

33

here as a continuous line. The "mix" consists of 50% Triton tholin and 50% amorphous carbon, each with a grain size of 6.3 µm. The H_2O ice grains are also 6.3 µm.

Figure 11. Three additional models of the spectrum of Titan in which all three components are spatially segregated from one another. W = H_2O ice, TT = Triton tholin, AC = amorphous carbon. The particle sizes are given in parentheses.

Figure 12. A model spectrum in which a 2% contribution from pure H_2O ice is added to the best-fitting mixture for the low-albedo material given in Figure 9.

Figure 13. The best model of the low-albedo hemisphere of Iapetus presented in this paper is shown with an extension to 5.5 µm wavelength in the upper panel. The "angularity" of the model results from the wide spacing of the wavelength sampling of the optical constants used in the calculations. In fact, the -C≡N fundamental absorption near 4.6 µm in the lower panel is quite sharp (McDonald et al. 1994; Khare et al. 1994b). This will be of use as new data at longer wavelengths become available, either from ground-based observations or from the VIMS (visible and infrared mapping spectrometer) on the Cassini spacecraft. For comparison, the lower panel shows our best re-computation of the preferred model by Wilson and Sagan (1995). For the latter, we show a version of the new data in which we have used a linear mixing model to correct for 10% contamination of the spectrum by the high-albedo hemisphere material (H_2O ice) as assumed by Wilson and Sagan (1996).
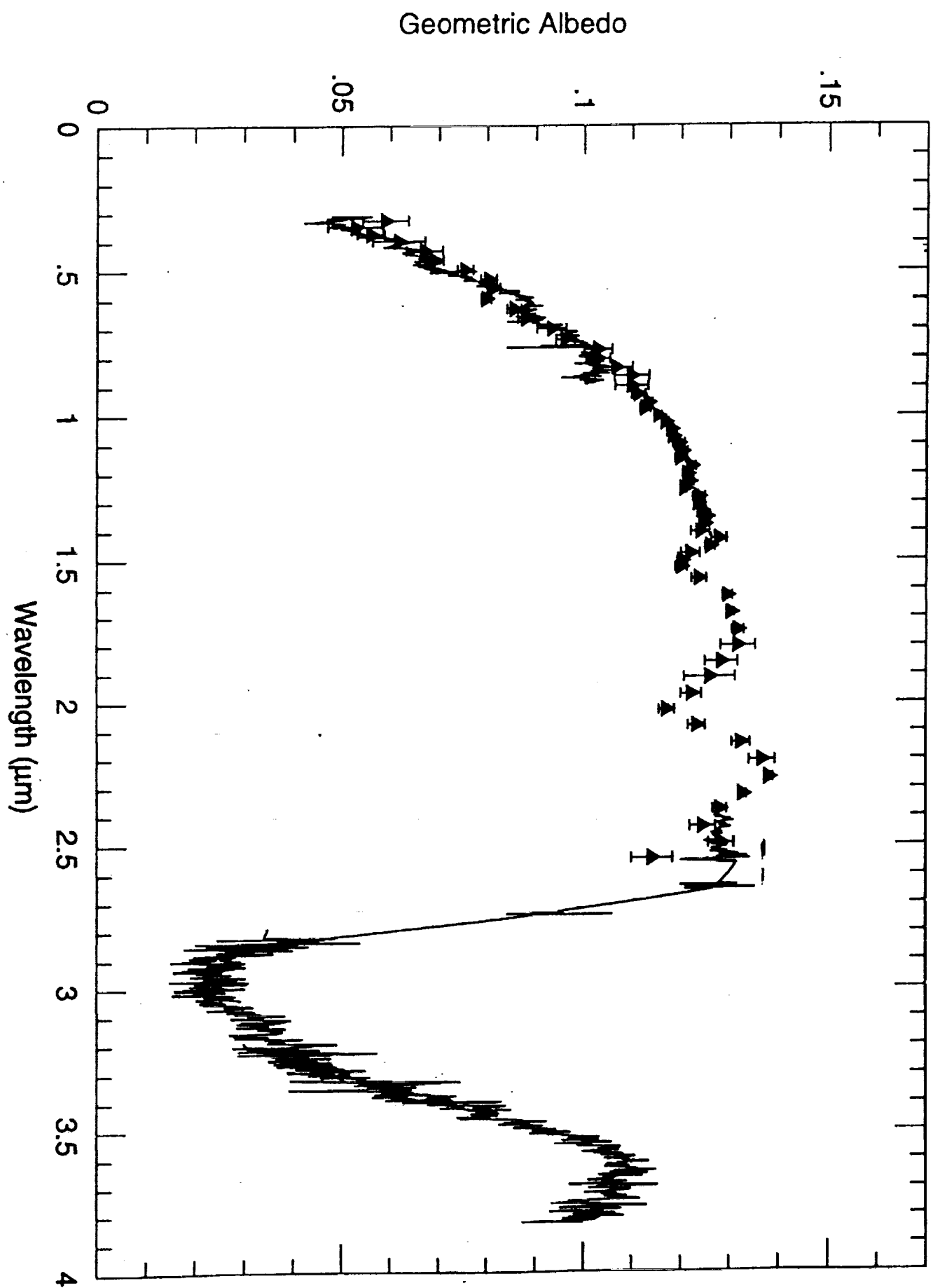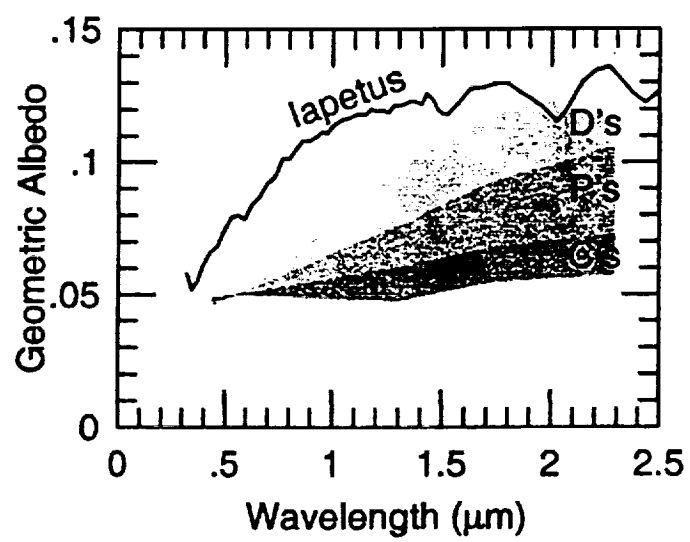
E-elongation (Leading)
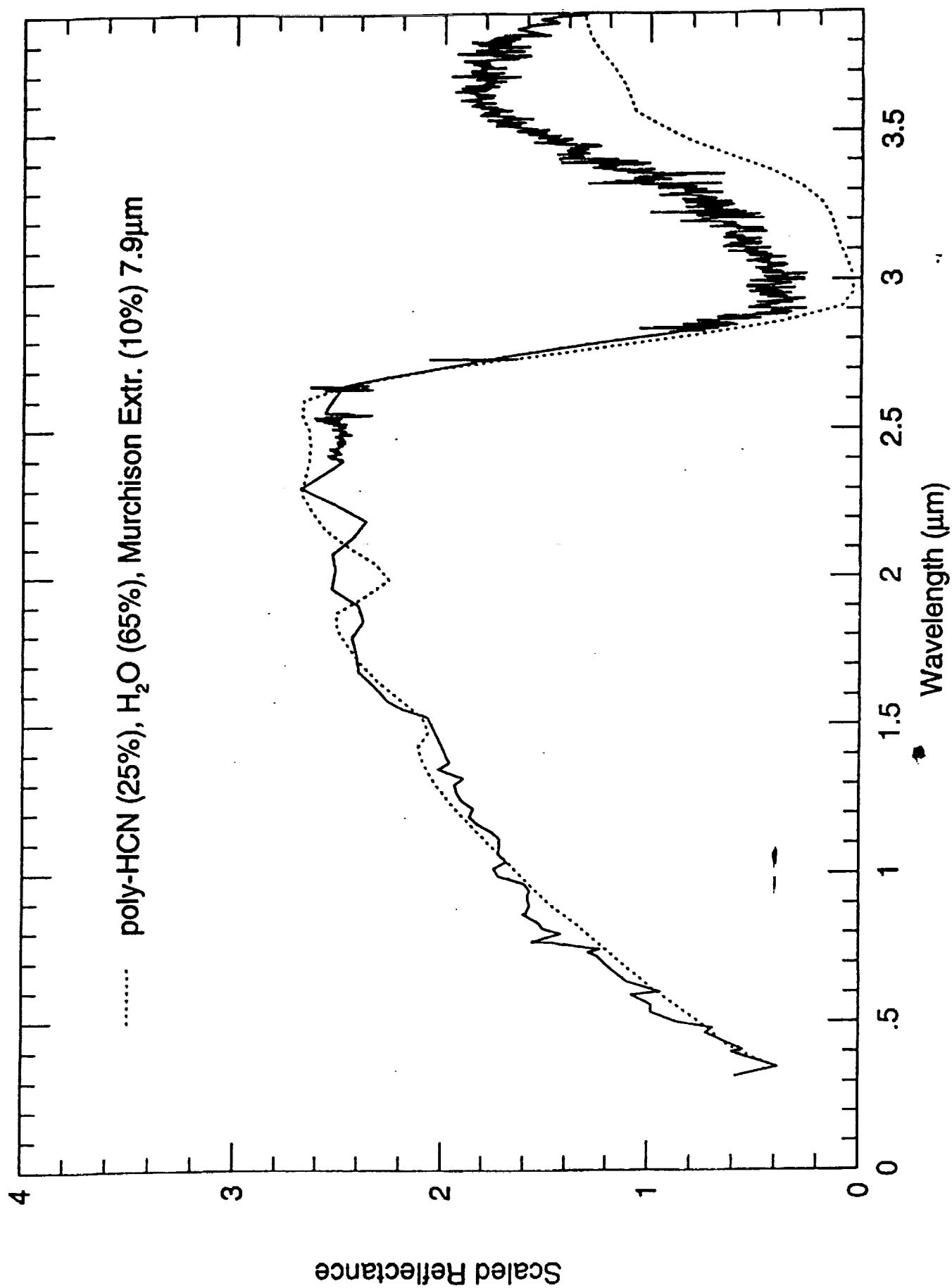1997 Oct 6

W-elongation (Trailing)
1998 Dec 18

Wavelength (μm)

Flux (10^{-16} W m^{-2} μm^{-1})

Figure 1.

Figure 2

Figure 3

poly-HCN (25%), H₂O (65%), Murchison Extr. (10%) 7.9µm

Scaled Reflectance

Wavelength (µm)

Figure 4

Figure 5

Hematite

Goethite

Jarosite

Iapetus

Reflectance

Wavelength (μm)

Figure 6

Geometric Albedo

Wavelength (μm)

H₂O (30%), Amorphous C (70%), 6.3μm

H₂O (40%), Amorphous C (60%), 6.3μm

H₂O (50%), Amorphous C (50%), 6.3μm

H₂O (60%), Amorphous C (40%), 6.3μm
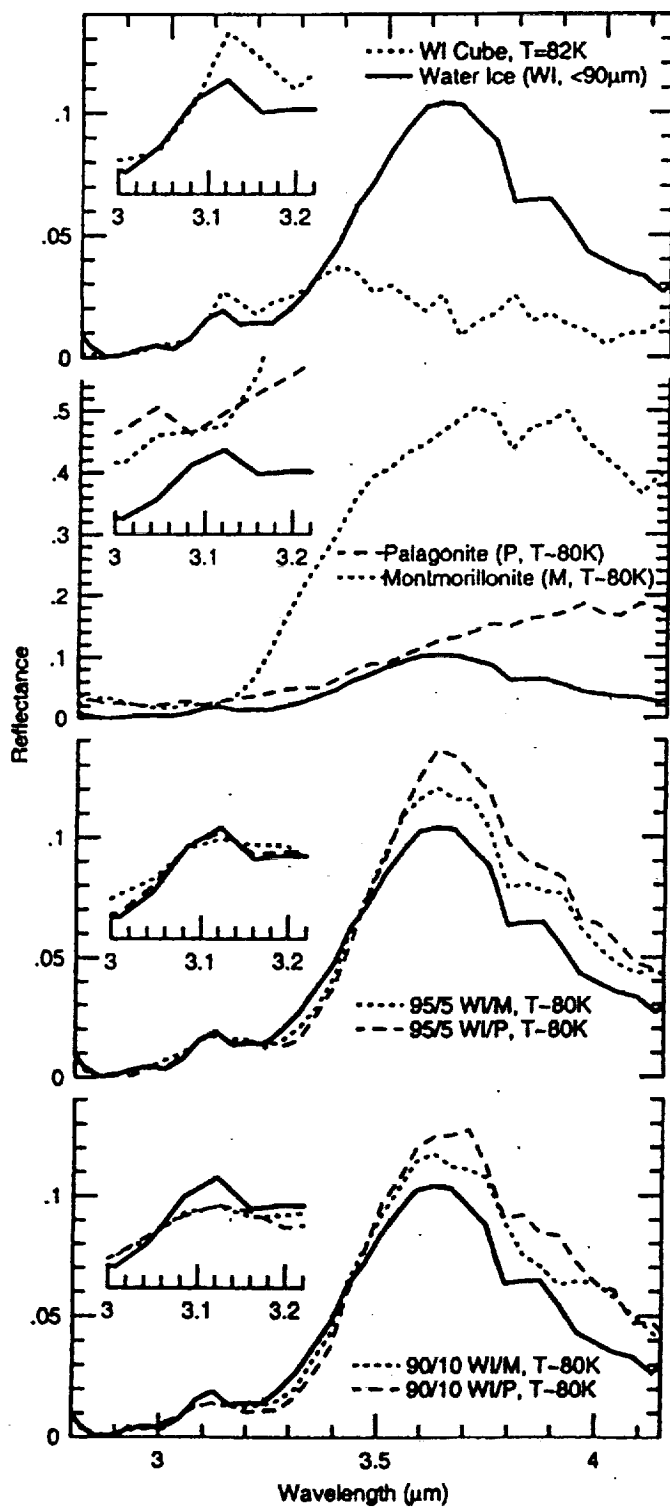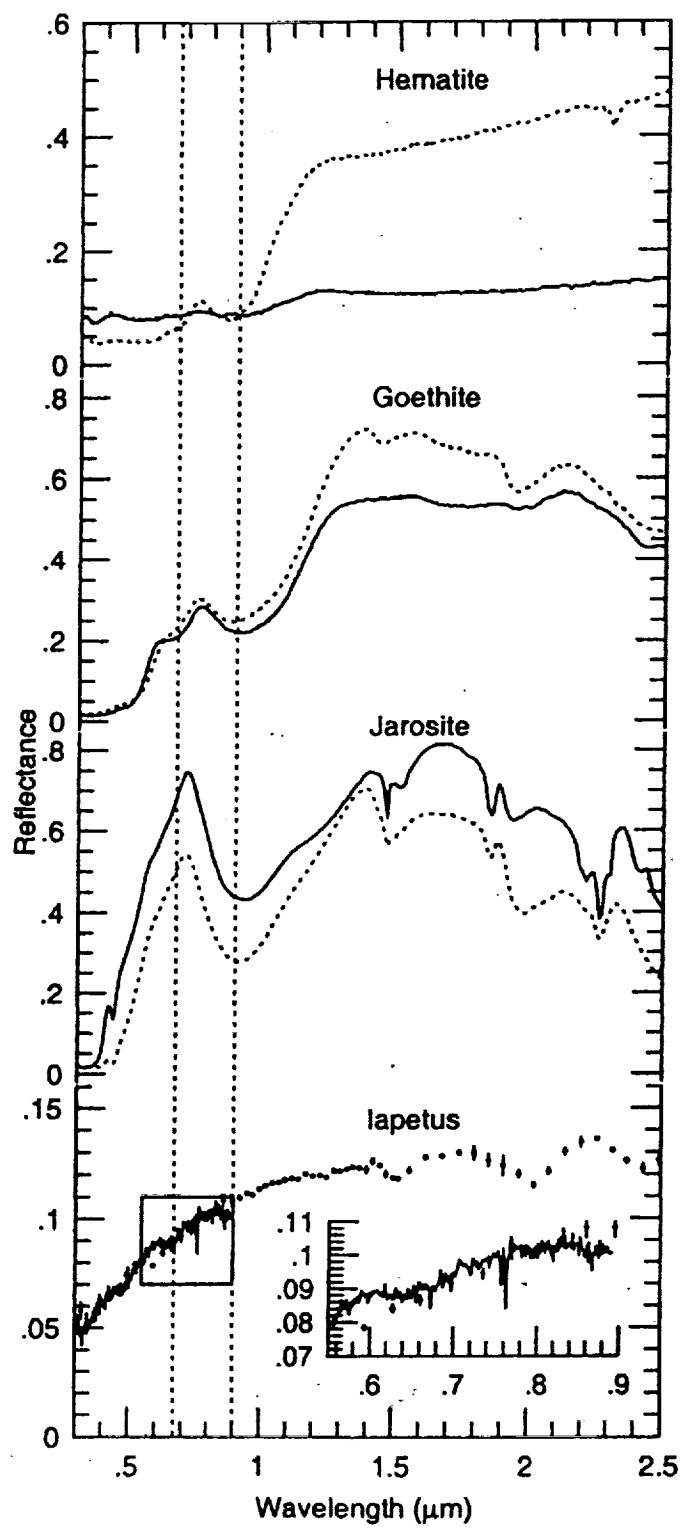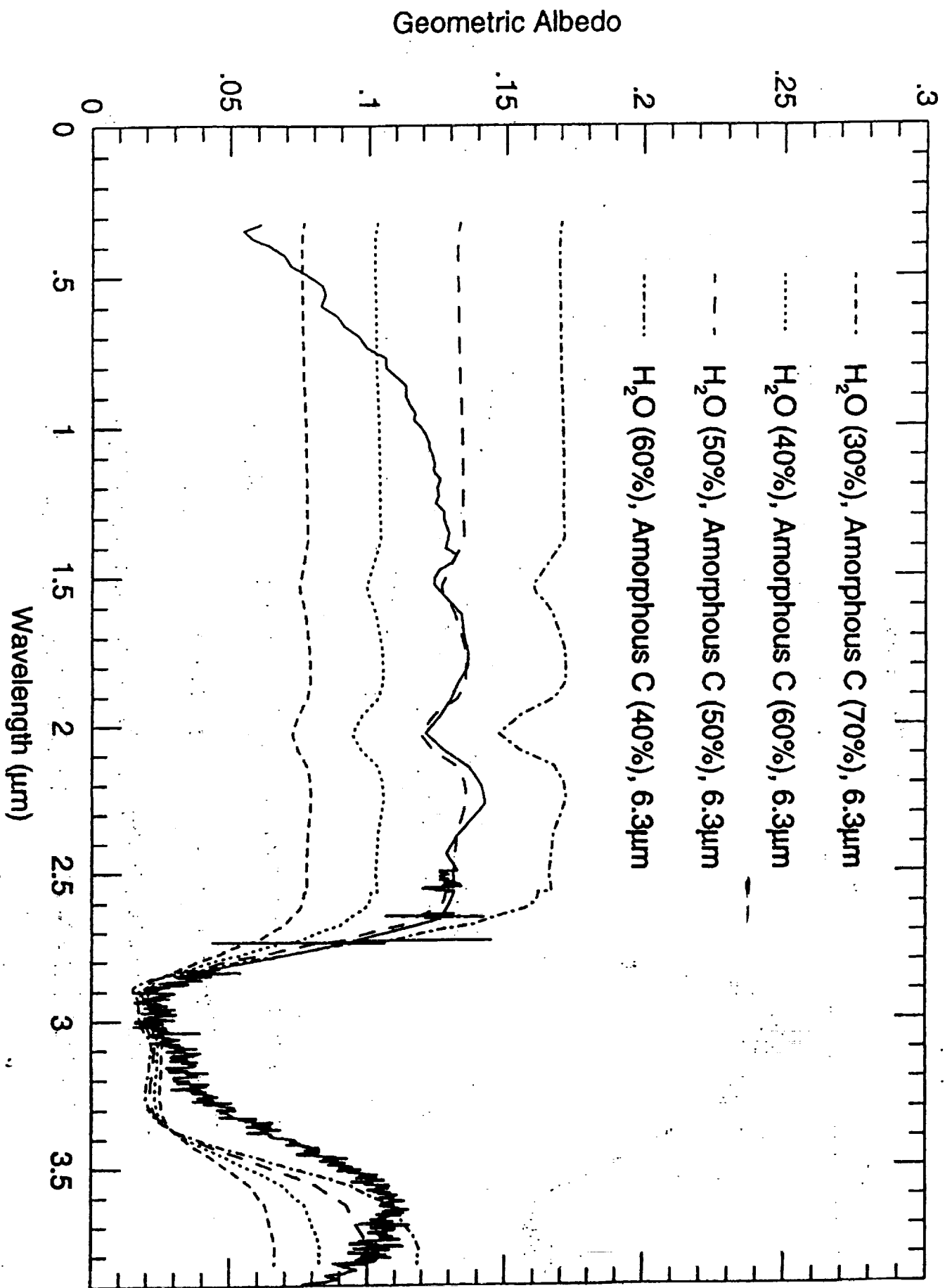
Figure 7

Figure 8

Geometric Albedo

Wavelength (μm)

- - H₂O (35%), Titan Tholin (25%), Amorphous C (40%), 6.3μm
····· H₂O (40%), Titan Tholin (20%), Amorphous C (40%), 6.3μm
— · — H₂O (20%), Titan Tholin (40%), Amorphous C (40%), 6.3μm
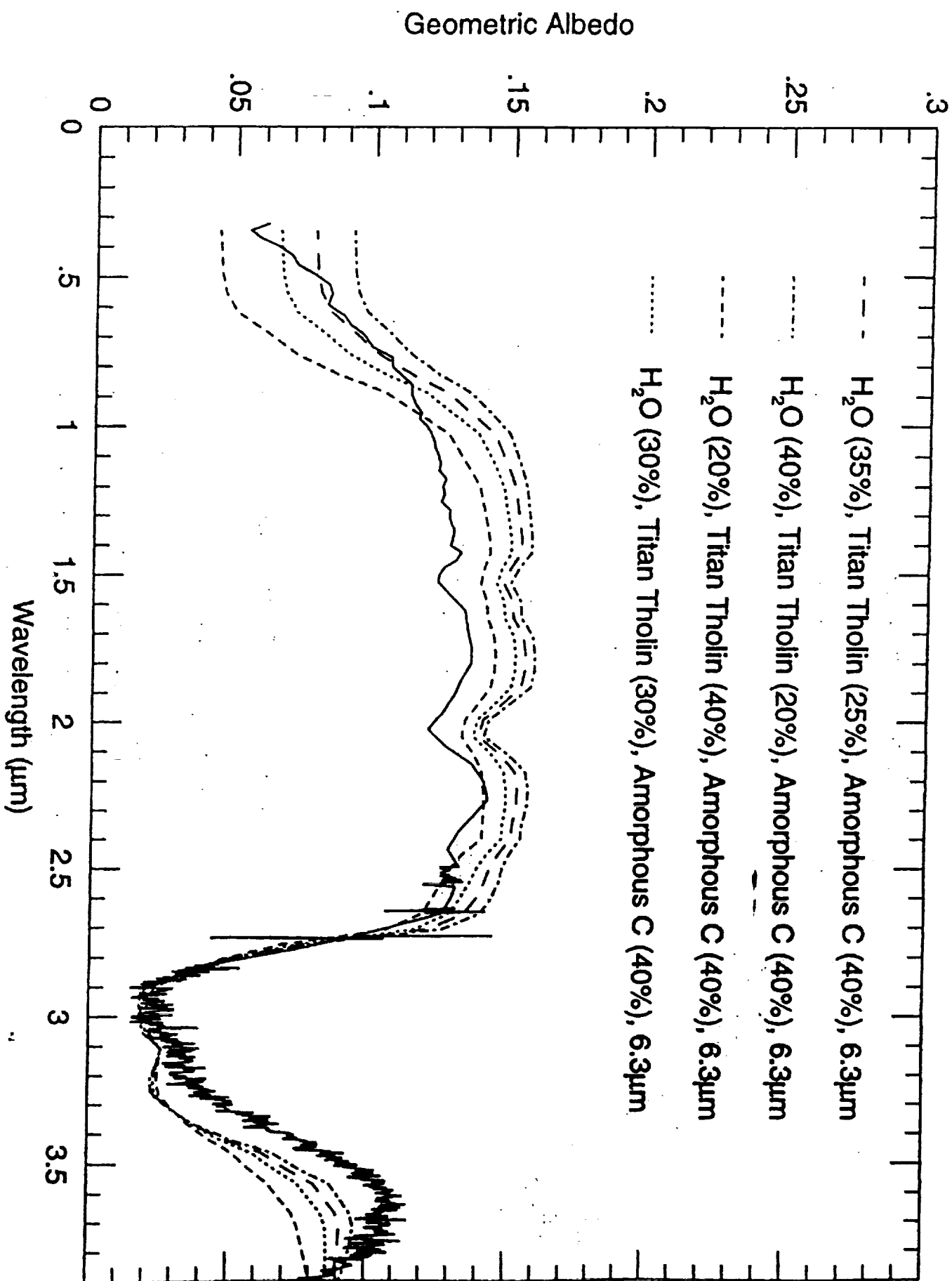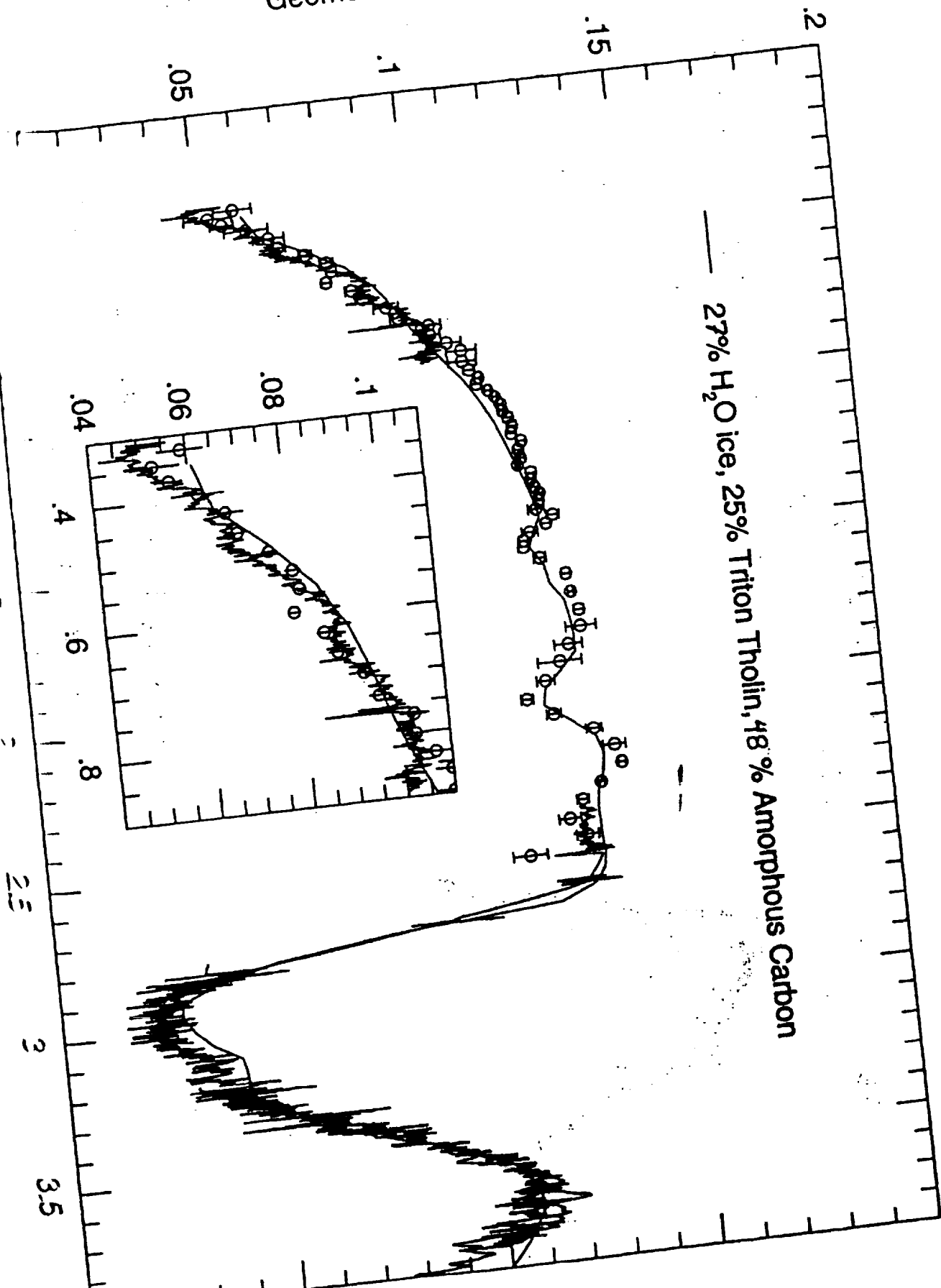– – H₂O (30%), Titan Tholin (30%), Amorphous C (40%), 6.3μm

Geometric Albedo

27% H₂O ice, 25% Triton Tholin, 48% Amorphous Carbon

Figure 10
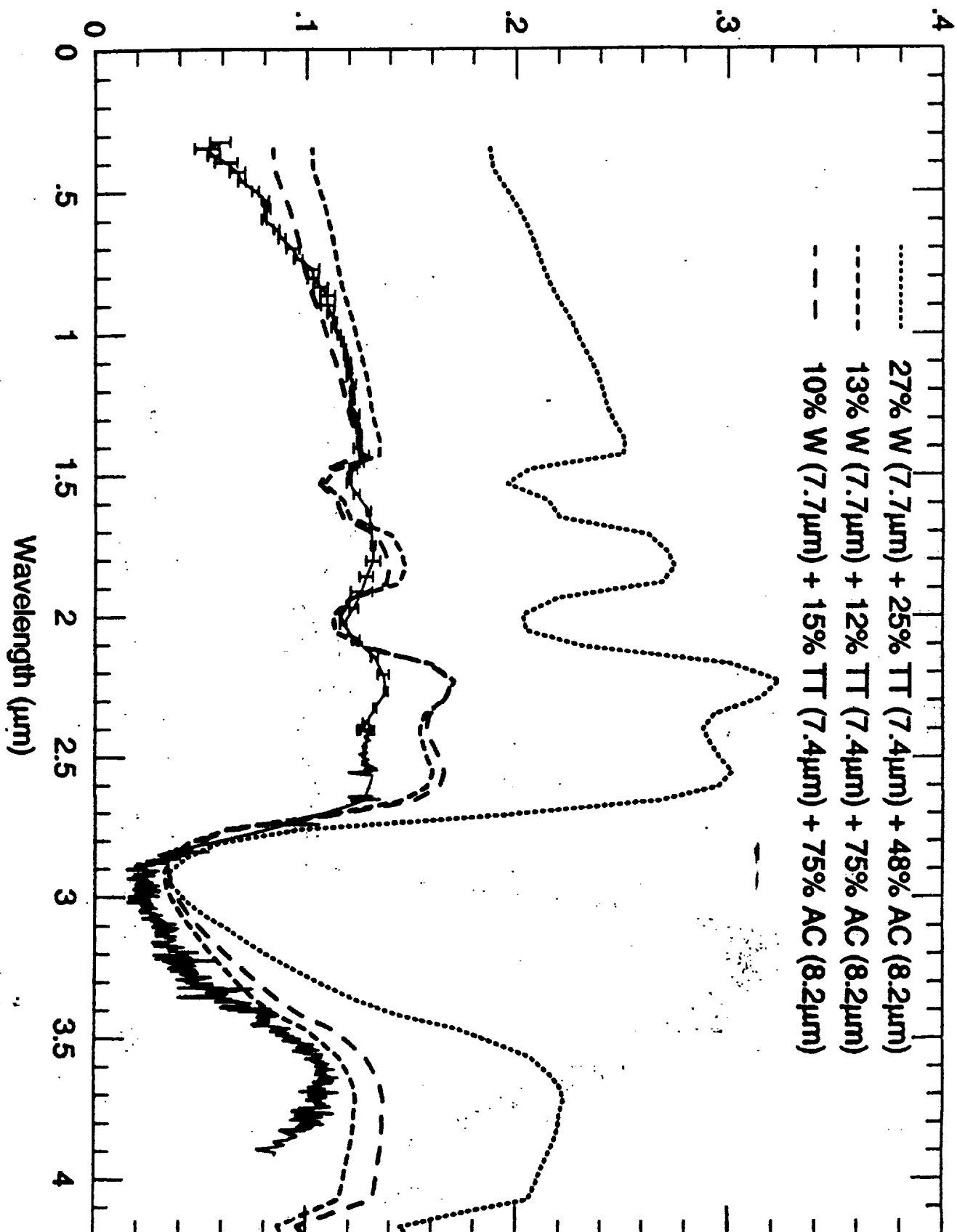
Figure 11
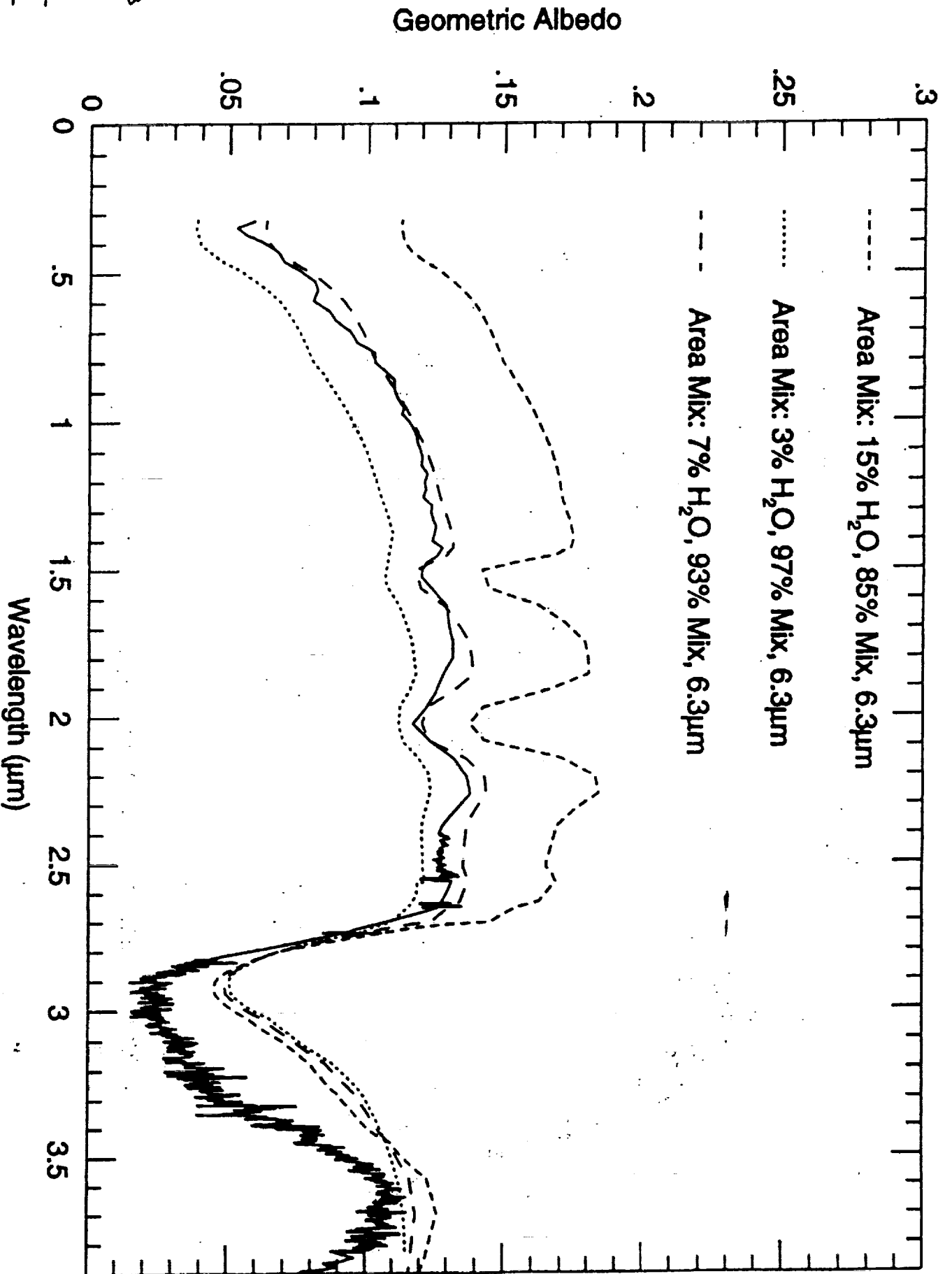
Geometric Albedo vs. Wavelength (μm)

Legend:
- ······ 27% W (7.7μm) + 25% TT (7.4μm) + 48% AC (8.2μm)
- — — 13% W (7.7μm) + 12% TT (7.4μm) + 75% AC (8.2μm)
- — — 10% W (7.7μm) + 15% TT (7.4μm) + 75% AC (8.2μm)

Geometric Albedo

Wavelength (μm)

Spatial Mixture:

98% [H₂O, Triton Tholin, Amorphous C]
2% [Pure H₂O Ice (100μm)]

Figure 12

27% H2O ice, 25% Triton Tholin, 48% Amorphous Carbon

——: Observations corrected for bright contribution

- - -: poly-HCN (25%), H2O (65%), Murchison Extr. (10%) 6.3μm

Geometric Albedo

Wavelength (μm)

Figure 13

Owen et al.